

# Analysis of the electronic delocalization in some $B_{12}$ 's isoelectronic analogues doped with beryllium and/or carbon

Rafael Islas,<sup>1,2</sup> Diego Inostroza,<sup>3</sup> David Arias-Olivares,<sup>1,4</sup> Bernardo Zúñiga-Gutiérrez,<sup>2</sup>  
Jordi Poater,<sup>5,6</sup> and Miquel Solà<sup>7</sup>

<sup>1</sup>Departamento de Ciencias Químicas, Facultad de Ciencias Exactas, Universidad Andres Bello, Av. República 275, Santiago, Chile

<sup>2</sup>Departamento de Química, Centro Universitario de Ciencias Exactas e Ingenierías, Universidad de Guadalajara, Blvd. Marcelino García Barragán 1421, C.P. 44430, Guadalajara, Jalisco, México.

<sup>3</sup>Doctorado en Físicoquímica molecular, Universidad Andres Bello, Av. República 275, Santiago, Chile

<sup>4</sup>Center of Applied Nanoscience (CANS), Facultad de Ciencias Exactas, Universidad Andres Bello, Av. República 275, Santiago, Chile

<sup>5</sup>Departament de Química Inorgànica i Orgànica & IQTCUB, Universitat de Barcelona, Martí i Franquès 1-11, 08028 Barcelona, Catalonia, Spain

<sup>6</sup>ICREA, Pg. Lluís Companys 23, 08010 Barcelona, Spain

<sup>7</sup>Institut de Química Computacional i Catàlisi (IQCC) and Departament de Química, Universitat de Girona, C/ Maria Aurèlia Capmany 69, 17003 Girona, Catalonia, Spain

Mail to: rafael.islas@unab.cl, bernardo.zuniga@academicos.udg.mx, miquel.sola@udg.edu

## Abstract

In the current work, a new family of isoelectronic analogues to  $B_{12}$  is reported. The construction of this family was performed through the isoelectronic substitution principle to generate species such as  $B_{11}C^+$ ,  $B_{11}Be^-$ ,  $B_{10}BeC$ ,  $B_{10}C_2^{2+}$ ,  $B_{10}Be_2^{2-}$ ,  $B_9Be_2C^-$ , and  $B_9BeC_2^+$ . The search for the global minimum was realized employing genetic algorithms, while the induced magnetic field, electronic localization function, magnetic current densities, and multicenter aromaticity criteria were calculated to understand their electronic delocalization. Our results show that, in general, C atoms avoid hypercoordination, whereas we have found species with Be atoms located in hypercoordinated positions that are relatively stable. Our analysis of aromaticity indicates that  $B_{12}$  has double  $\sigma$  and  $\pi$  disk aromaticity. Mono, double or triple substitution of B by  $C^+$  or  $Be^-$  reduces somewhat the aromaticity of the clusters, but less in the case of  $Be^-$  substitution.

**Keywords:**  $B_{12}$ ; electronic delocalization; ELF; MCI; MICD; induced magnetic field; chemical transmutation; aromaticity; boron cluster.

## 1. Introduction

In 1988, Anderson et al. observed an intense signal associated to  $B_{13}^+$ , a very stable boron cluster in comparison with other boron clusters of similar size.<sup>1</sup> The dissociation of  $B_{13}^+$  in  $B_{12} + B^+$  occurs more easily compared to other dissociations leading to  $B_n^+$  compounds. This low-energy dissociation indicates a high stability of the  $B_{12}$  cluster. The global minimum of this neutral system is a bowl-shaped molecule (see Figure 1), but despite its non-planar geometry it has been classified as an aromatic compound.<sup>2</sup> There are three different types of B atoms in  $B_{12}$  as shown in Figure 1. Kiran et al. stated that 18 out of the 36 valence electrons in  $B_{12}$  are localized in the B-B single bonds, forming the outside  $B_9$  ring; while the inner-ring,  $B_3$ , is formed by 6  $\sigma$  electrons. And the remaining 12 valence electrons are divided in two groups: first, 6  $\pi$  electrons are delocalized in the entire  $B_{12}$ , and, on the other hand, 6  $\sigma$  electrons are delocalized between the inner- and the outside rings.<sup>2</sup>

$B_{12}$  cluster presents three different boron atoms: two in the external ring and the third one in the internal ring, as depicted in Figure 1. The difference between position 1 and position 2 is the chemical environment: boron 1 atoms are surrounded by three other B atoms, whereas boron 2 atoms are surrounded by four atoms. Boron atoms 3 are surrounded by six B atoms.

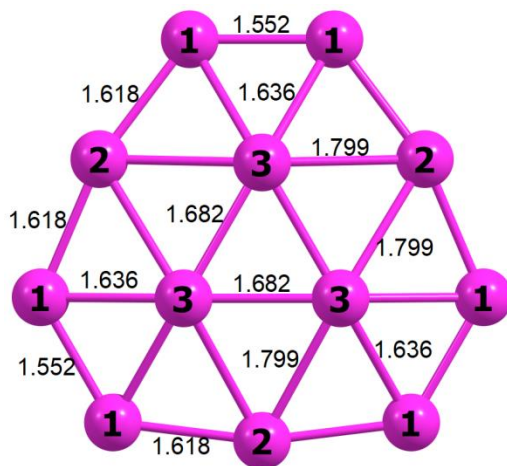


**Figure 1.** The global minimum of the  $B_{12}$  cluster is a bowl-shaped structure ( $C_{3v}$ ). The labels on the spheres represent the three positions in the  $B_{12}$ . The bond length distances are in Å.

Many boron compounds present a (quasi-)free internal rotation (best example is  $B_{19}^-$ ),<sup>3</sup> but  $B_{12}$  cluster presents an umbrella-inversion instead of internal rotation.<sup>4</sup> Furthermore, many of the boron clusters are stabilized by both  $\pi$ - and  $\sigma$ -electronic delocalization. The electron deficiency in the boron atom forces the multicenter bonding. On the other hand, beryllium also exhibits electron deficiency, with two valence electrons. However, compared with the widely studied boron chemistry, the number of beryllium systems synthesized to date is scarce. This is probably due to the high toxicity of the beryllium.<sup>5</sup> Also similar to boron, beryllium has been employed to stabilize aromatic systems through hypercoordinated atoms.<sup>6</sup> In the current work, boron atoms in  $B_{12}$  are replaced by the cation  $C^+$  or the anion  $Be^-$ , both chemical entities with 3 valence electrons. The main goal of this work is to study the changes in the molecular and electronic structure of  $B_{12}$  when one or more boron atoms are substituted by their isoelectronic analogues, i.e.  $C^+$  cation and/or  $Be^-$  anion. This procedure has been called electronic transmutation.<sup>7-8</sup> If the beryllium atom is an electron-deficient atom, such as the boron atom, what is the electronic structure of a boron cluster doped with this element? Should it be similar? At difference, carbon is not electron-deficient, thus should the carbon-doped boron clusters behave differently? Are the properties of  $B_{12}$  more affected by  $Be^-$  or  $C^+$  substitution?

All the new molecules proposed in this work also contain 36 valence electrons, like  $B_{12}$ , and their electronic delocalization is analyzed in terms of the induced magnetic field (or  $\mathbf{B}^{ind}$ ),<sup>9</sup> electronic localization function (ELF),<sup>10</sup> and multicenter aromaticity criterion.<sup>11-13</sup> The  $\mathbf{B}^{ind}$  has already been employed with the aim of understanding the electronic delocalization of other boron clusters,<sup>14-16</sup> and in some other molecules generated by isoelectronic

substitutions.<sup>17-18</sup> Plots of the  $\mathbf{B}^{\text{ind}}$  have been also employed in some containing-beryllium clusters.<sup>19</sup> In particular, the  $B_{12}$  isoelectronic analogues under analysis are:  $B_{11}C^+$ ,  $B_{11}Be^-$ ,  $B_{10}C_2^{2+}$ ,  $B_{10}Be_2^{2-}$ ,  $B_{10}BeC$ ,  $B_9Be_2C^-$ ,  $B_9BeC_2^+$  and finally, for comparison, the totally boron-free  $Be_6C_6$ .

## 2. Computational Details

The global minima (GM) search was done employing the GEGA algorithm proposed by Alexandrova.<sup>20</sup> Calculations have been performed with the PBE0<sup>21-22</sup> exchange-correlation functional and the LANL2DZ basis set. All optimizations were performed in the singlet state, as we checked that triplet states are always higher in energy by at least 25 kcal/mol at PBE0//def2-TZVP level. The ten most stable isomers were re-optimized employing the same PBE0 functional but employing the larger def2-TZVP basis set.<sup>23</sup> All geometries were characterized by frequency calculations and they were minima in their respective potential energy surfaces (PES's). The energy values of selected isomers were refined with CCSD(T)<sup>24</sup> methodology on the PBE0/def2-TZVP optimized geometries. The wave functions stabilities of the clusters proposed here were analyzed at PBE0/def2-TZVP level. Also the T1 analysis was performed for all the structures.<sup>25</sup> All these calculations (included the shielding tensors) were realized with Gaussian 09 program.<sup>26</sup> ELF was computed with deMon2k package<sup>27</sup> at PBE0/DZVP. The visualization of the isolines was realized with VisIt program.<sup>28</sup> The topological analysis (included the images) was performed with MultiWFN program.<sup>29</sup> Aromaticity was evaluated at the PBE0/def2-TZVP level of theory by means of the multicenter electron sharing indices (MCI),<sup>11-13</sup> the electron localization function,<sup>10</sup> the induced magnetic field ( $\mathbf{B}^{\text{ind}}$ ),<sup>9</sup> and the magnetically induced current density (MICD).<sup>30</sup> MCIs provide a measure of electron sharing among the atoms considered. We also calculated

delocalization indices (DIs), which are two-center electron sharing indices (i.e., two-center MCIs) that measure electron sharing between two atoms. Although several partitions can be used to define the atomic regions needed to calculate DIs and MCIs,<sup>31</sup> we made use of the molecular partition based on the quantum theory of atoms in molecules (QTAIM). MCI and DI indices were obtained with the ESI-3D program.<sup>32-34</sup>

The magnetically induced current density (MICD) has been obtained in the framework of DIRAC17 program,<sup>35</sup> with the calculations carried out employing the functional B3LYP.<sup>36-38</sup> The 4-component Dirac-Coulomb Hamiltonian has been employed,<sup>39</sup> in conjunction with the cc-pVDZ basis set.<sup>40-41</sup> The magnetic field vector is placed perpendicularly to the molecular plane. Once the linear response to the perturbing magnetic dipole is obtained, the result was used to construct the first-order current density. The integration of the MICD was done using the two-dimensional Gauss-Lobatto quadrature where the plane was extended from the molecular centre to  $15 a_0$ . The integration is reported as the sum of its components ( $x+y+z$ ). The stream plots were done using PyNGL,<sup>42</sup> where the circles represent the atomic positions and the line intensity is proportional to the norm of the current density vector. Two different planes are presented, the molecular plane and 1 a.u. above the molecular plane.

### **3. Results and discussion**

#### **3.1. Structural details**

##### **3.1.1. One-atom substitution**

Figure 2 encloses the global minima structures of the mono-substituted isoelectronic isomers to B<sub>12</sub>. B<sub>12</sub> has been labeled as **1**, whereas its first isoelectronic analogue, in which one B was replaced by one C<sup>+</sup>, is labeled as **2**. The global minimum (GM) structure found for **2**, in which B in position 1 is substituted by C<sup>+</sup>, is quite similar to the original structure **1**. Enantiomers

for **2** have also been detected, both with a bowl-shaped structure of  $C_1$  symmetry. The next closest energetic isomer of **2**, labeled as **21** (Figure 2), is 20 kcal mol<sup>-1</sup> less stable than **2**, with the carbon atom also placed in the external ring, but in position 2. Something similar was previously observed for the neutral B<sub>18</sub>C, which is the neutral isoelectronic analogue of B<sub>19</sub><sup>-</sup>.<sup>43</sup> The GM of B<sub>19</sub><sup>-</sup> is a planar double concentric ring structure, with the external ring formed by 13 boron atoms surrounding a pentagon formed by 6 boron electrons;<sup>44</sup> whereas the GM of B<sub>18</sub>C is also similar to the planar B<sub>19</sub><sup>-</sup> structure, with the carbon atom lying in the external ring. Finally, the lowest energy isomer of **2** substituted in position 3 is 33 kcal/mol higher in energy (Supporting Information).

Next, if one B of **1** is replaced by one Be<sup>-</sup> in position 2 (structure **3**, Figure 2), the GM structure adopted is the same as the original B<sub>12</sub>, with the beryllium atom placed in the external ring. The next energetic isomer is 10 kcal mol<sup>-1</sup> less stable (labeled as **31**, Figure 2), in which the beryllium atom emigrated from the external to the internal ring (at position 3), being surrounded by six boron atoms. Kang et. al found other GM for B<sub>11</sub>Be<sup>-</sup> but the results in the current work showed that isomer is less stable by 16 kcal/mol than **3** at CCSD(T)//def2-TZVP level on structures optimized at PBE0//def2-TZVP.<sup>45</sup> And for completeness, the lowest energy isomer of **3** substituted in position 1 is 12 kcal/mol less stable than **3**.



### 3.1.2. Two-atoms substitution

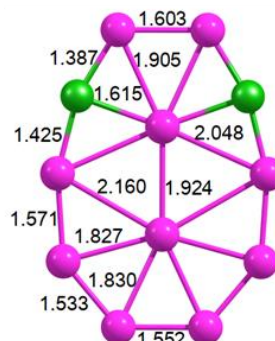
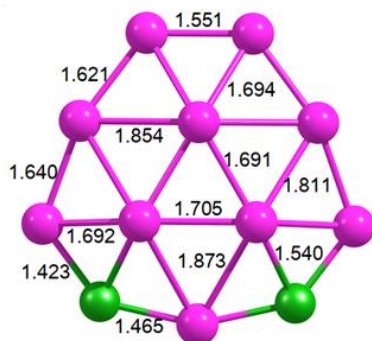
Figure 3 encloses the double-replaced analogues; thus, two boron atoms were replaced by either two  $C^+$  cations (**4**, 11 substitution), two  $Be^-$  anions (**5**, 22 substitution), or one  $Be^-$  anion and one  $C^+$  cation (**6**, 13 substitution). As can be seen,  $C^+$  prefers to be located at position 1, whereas  $Be^-$  favors positions 2 or 3. This result concurs with the previously reported finding by Boldyrev et al. that carbon tends to avoid hypercoordination in  $CB_6^-$ ,  $CB_6^{2-}$ , and  $C_2B_5^-$  planar carbon-boron clusters.<sup>46</sup> For the double-carbon substitution, the global minimum presents a similar structural skeleton to **1**, with the two carbon atoms lying in the external ring. The two carbons prefer not to form a C-C bond, but they are separated by one boron atom. The 2 kcal mol<sup>-1</sup> less stable isomer **41** consists of a 9-membered ring with two boron atoms placed in the center of the ring. Next, if the substitution is done with two beryllium anions, the GM (**5**, 22 substitution) also presents the geometry of  $B_{12}$ , with the two Be atoms placed in the external ring, as well as for the next energetically isomer (**51**, 12 substitution). Finally, **6** (13 substitution) is the GM when one carbon and one beryllium are introduced. In this case, the C atom is localized in the external ring, bonded to the Be atom located in the center of a six-membered ring formed by five boron atoms and the carbon atom. The next stable isomer (**61**, 12 substitution) is just 1 kcal/mol higher in energy, and both C and Be are localized in the external ring, forming a C-Be bond. Both **6** and **61** could coexist due the small energetic difference.

SYSTEM

GLOBAL MINIMUM

NEXT ISOMER

$B_{10}C_2^{+2}$

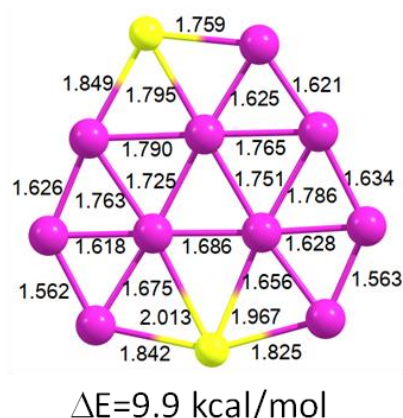
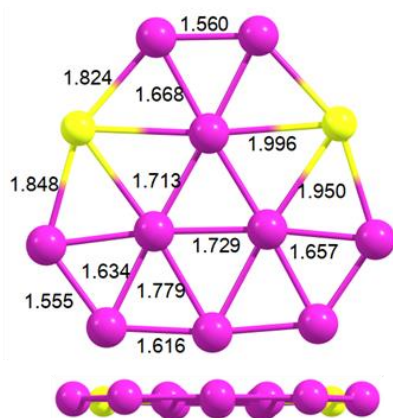


$\Delta E=2.3$  kcal/mol

4

41

$B_{10}Be_2^{-2}$

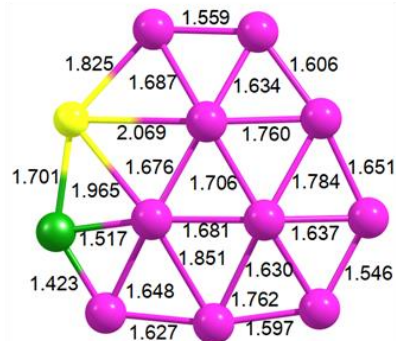
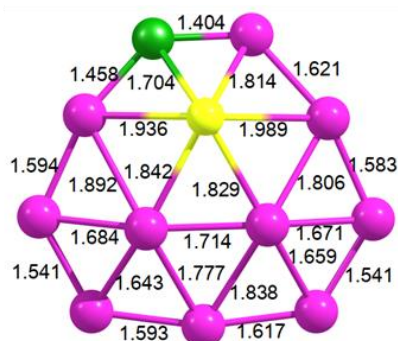


$\Delta E=9.9$  kcal/mol

5

51

$B_{10}CBe$



$\Delta E=1.1$  kcal/mol

6

61

**Figure 3.** The two-atoms substitution on B<sub>12</sub>. In this stage two B atoms were replaced by two C<sup>+</sup>, by two Be<sup>-</sup> or by one C<sup>+</sup> and one Be<sup>-</sup>. The bond length distances are in Å. The energetic difference ( $\Delta E$ ) between the lowest energetic isomer (Global Minimum or GM) and the next energetic isomer is reported and its units are kcal/mol. Only for GMs, a lateral view is depicted. The pink, green, and yellow spheres represent the boron, carbon, and beryllium atoms, respectively.

### 3.1.3. Three-atoms substitutions (and the complete B-B by C-Be substitution)

In the last stage, three boron atoms of **1** were replaced by either C<sup>+</sup>, Be<sup>-</sup> or both. There are four possible three-atom substitutions but the substitutions by three Be<sup>-</sup> or three C<sup>+</sup> is not considered here because they lead to highly charged unrealistic species. For the other two possible substitutions, in the first case, one Be<sup>-</sup> anion and two C<sup>+</sup> cations were introduced (**7**), with a different geometry to that of B<sub>12</sub>, in contrast to the next isomer (**71**), which is less stable by 1 kcal/mol. In **7**, the two C atoms are located in the external ring and Be in the central, whereas in **71** the three atoms are located in the external one (121 substitution). In the second case, one C<sup>+</sup> cation and two Be<sup>-</sup> anions were introduced (**8**), with the three atoms placed in the external ring (122 substitution). The 9 kcal/mol less stable isomer (**81**, 123 substitution) just consists of the exchange of one Be by one B atom in the central ring, both of them keeping the geometry of B<sub>12</sub>. Finally, and just introduced for comparison, **9** is the most stable isomer of a beryllium-carbon cluster, in which all B-B bonds in B<sub>12</sub> were converted into C-Be bonds; adopting a different geometry to that of B<sub>12</sub>. Interestingly, in **9**, C prefers external positions whereas Be is located preferentially in internal positions.

As a whole, geometrically, we observe how the substitution of B by C<sup>+</sup> keeps the bowl-shaped geometry (isomers **2** and **5**) of B<sub>12</sub>, whereas the substitution of B by Be<sup>-</sup> converts it into planar (isomers **3** and **6**). The reason can be found in the strain caused by the shorter B-C bond length compared to that of longer B-Be. For instance,  $r(\text{B}_1, \text{B}_1)$  and  $r(\text{B}_1, \text{B}_2)$  in **1** are 1.552 and 1.618 Å, respectively, which are shortened to 1.424 and 1.483 Å in **2**,

respectively, thus keeping the bowl-shaped geometry. On the other hand,  $r(\text{B}_1, \text{B}_2)$  and  $r(\text{B}_2, \text{B}_3)$  in **1** are 1.618 and 1.799 Å, respectively, which are elongated to 1.856 and 1.981 Å in **3**, respectively, thus allowing a planar geometry. A planar geometry is preferred to favor electron delocalization, but if bonds are too short there is no way to avoid introducing curvature in the molecular structure. As to the position occupied by  $\text{C}^+$  or  $\text{Be}^-$ ,  $\text{C}^+$  is more electronegative than  $\text{Be}^-$  and, consequently, this cation tends to prefer positions with localized 2c-2e bonds, i.e., those found in the external ring frame. For  $\text{Be}^-$ , the preference for external positions is less strong.



**Figure 4.** The three-atoms substitution on  $B_{12}$  considered. Two B atoms were replaced by two  $C^+$  and one B atom by one  $Be^-$ , or two boron atoms by two  $Be^-$  and one B atom by  $C^+$ . The structure of  $C_6Be_6$  is also given. The bond length distances are in Å. The energetic difference ( $\Delta E$ ) between the lowest energetic isomer (Global Minimum or GM) and the next energetic isomer is reported and its units are kcal/mol. Only for GMs, a lateral view is depicted. The pink, green, and yellow spheres represent the boron, carbon, and beryllium atoms, respectively

### 3.2 Topological Analysis

As an attempt for a better comprehension of the electronic structure of the clusters, a topological analysis of the electronic density was performed employing Bader's *Atoms In Molecules* (AIM) approach.<sup>47</sup> Critical points of the nine GM structures proposed in the current work are depicted in Figure 5. The pink, orange, and yellow colored dots represent the atomic critical points (ACPs), the bond critical points (BCPs), and the ring critical points (RCPs), respectively. In all compounds, the number of ACP's correctly correspond with the number of atoms and symmetry of the compounds. The orange lines represent the bond paths, which are the paths of maximum electron density.

First, in cluster **1**, we observe the expected nine and three BCPs in the external  $B_9$  and inner  $B_3$  rings, respectively. However, only three BCPs of the external ring are connected with three inner boron atoms (ACPs), forming three ACP-BCP interactions. This latter translates into four RCPs, one in the center of the  $B_3$  ring, and the other three distributed between the internal and external rings. So, the number of RCPs differs from the expected twelve by considering all three-membered boron rings (Figure 5). This pattern is in a good agreement with the previous work of Kiran et. al.<sup>2</sup>

The AIM topological representations for clusters **2-5** are very similar to that of  $B_{12}$  (Figure 5). Thus, in all cases we obtain four RCPs, i.e. the one in the center and three between the  $B_9$  and  $B_3$  rings. However, when we have C atoms in the cluster, the three bond paths that connect these two rings differ from **1**. In particular, we observe a bond path connecting an

inner B and the C, i.e. a B-C bond, one in **2** and two in **4**. In contrast, when either one (**3**) or two Be (**5**) are introduced, we have the same bond paths connecting the inner B atoms with three external BCPs, so AIM shows no B-Be bond for the internal B atoms.

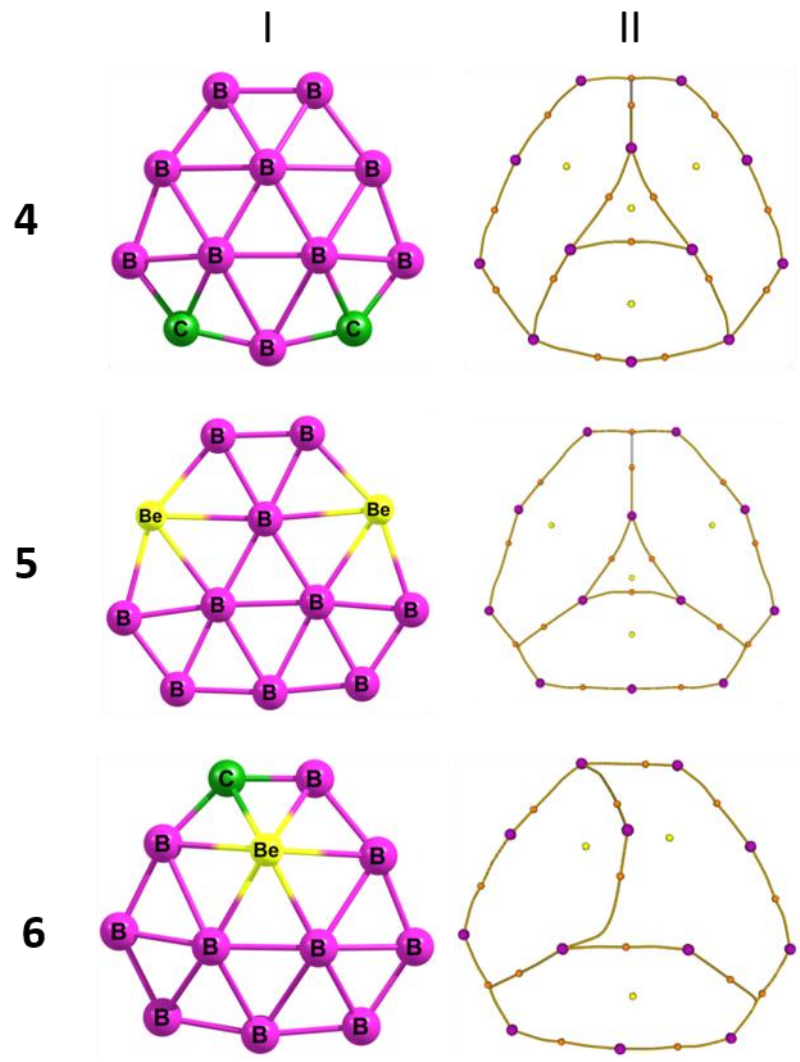
System **6** presents a carbon in the external ring and a beryllium in the inner ring (Figure 5). According to the AIM analysis, the three internal atoms (Be, B, and B) do not form a ring because there is no BCP between one B and the Be<sup>-</sup> and, as a consequence, presents one RCP less in comparison with the systems previously discussed, *i.e.* **6** has only three RCPs. The Be is connected to the C via ACP-ACP interaction.

Cluster **7** is similar to previously studied B<sub>11</sub><sup>-</sup> cluster, which is called “molecular tank”.<sup>48</sup> It is formed by an external 10-membered ring (including two C atoms) and two internal atoms (B and Be). Again, the AIM analysis shows that Be is connected to the two C atoms via two ACP-ACP interactions, like for **6**. On other hand, the inner B is united to external ring via one ACP-ACP (possible B-B bond) and ACP-BCP interactions. There are also four RCPs in this compound.

In cluster **8**, the introduced two Be and the C ions are placed in the external ring, with a similar shape to initial B<sub>12</sub>. At difference with above discussed systems, the internal atoms present only two BCPs, preventing the formation of a RCP. As a consequence, there are three RCPs. Like for systems **3** and **5**, Be atoms do not present any bond path to the inner ring, whereas we do observe the B-C one, like for **2** and **4**. And the other two internal boron atoms are connected to two different BCPs, forming two ACP-BCP interactions.

As a whole, in terms of the topological analysis via AIM, it could be deduced certain similar bonding pattern in all the compounds, except for those containing simultaneously C and Be atoms (compounds **6**, **7**, and **8**), in which the inner ring does not have three BCPs any longer, and thus one RCP is lost. Nonetheless, it must be pointed out that it has been previously





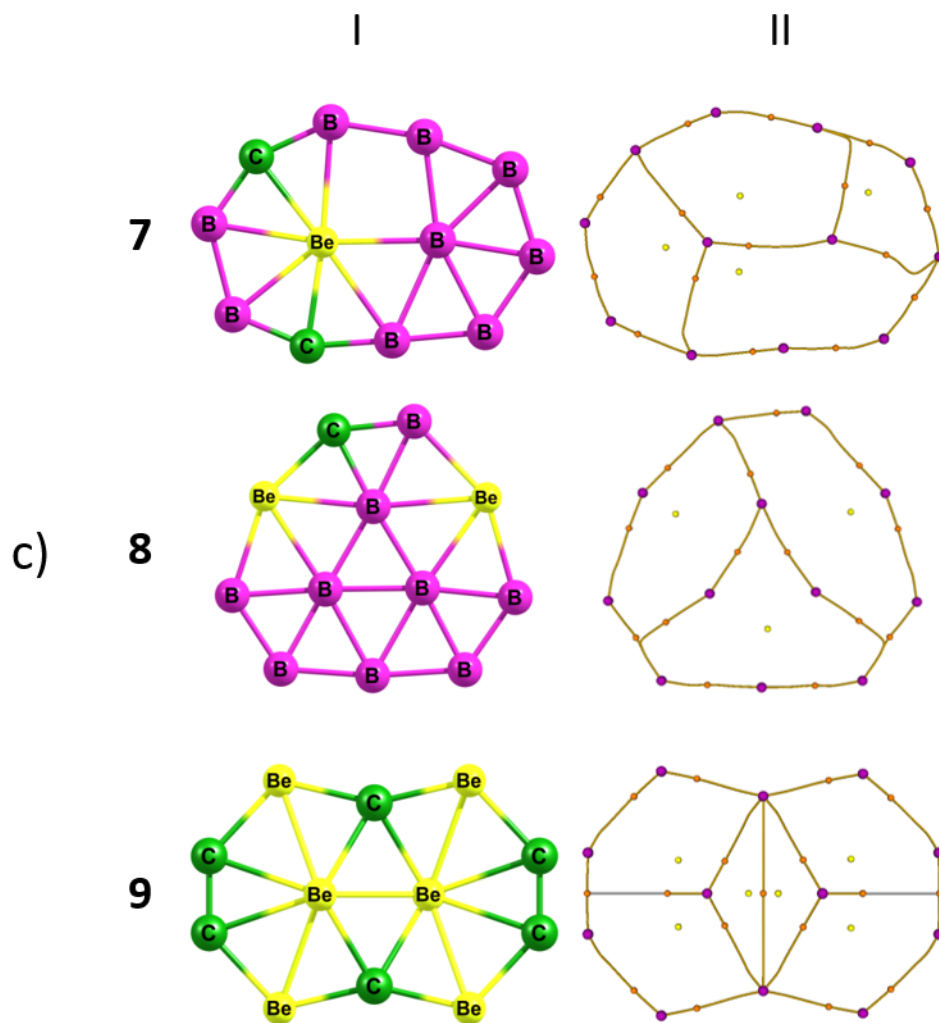


**Figure 5.** AIM's critical points. The molecular representations are shown in column **I** while the critical points together with the bond paths are shown in column **II**. The violet, orange, and yellow dots represent atomic critical points (ACP) (3,-3), bond critical points (BCP) (3,-1), and ring critical points (RCP) (3,+1), respectively. In **a**) the original cluster (**1**) is shown and the mono-substituted clusters **2** and **3**. In **b**) the double-substituted clusters (**4**, **5**, and **6**) are depicted, and finally, in **c**) the triple-substituted clusters (**7** and **8**) and the boron-free cluster (**9**) are shown.

The above topological analysis has been complemented by the delocalization indices (DIs) of the systems depicted in Figure 6. The  $DI(B,B)$  values close to 1.0 a.u. indicate the presence of a localized single B-B bond. And it can be observed that all the structures reported as GM present  $DI(B,B)$  (or  $\delta(B,B)$ ) values close to 1.0 a.u. in their external rings. In case of the central ring, those systems with a three-boron-ring,  $DI(B,B)$  are in the range 0.54 – 0.80 a.u.; as each of these B atoms are coordinated to more atoms, i.e. more delocalized. DIs show a clear different behavior between B-C (systems **2** or **4**) and B-Be (systems **3** and **5**) connecting external and inner rings. So, whereas  $\delta(B,C)$  is in the order 1.02 – 1.06 a.u.,  $\delta(B,Be)$  only amounts to 0.16 – 0.18 a.u., and this behavior perfectly correlates with the presence or absence of BCP discussed above in Figure 5.

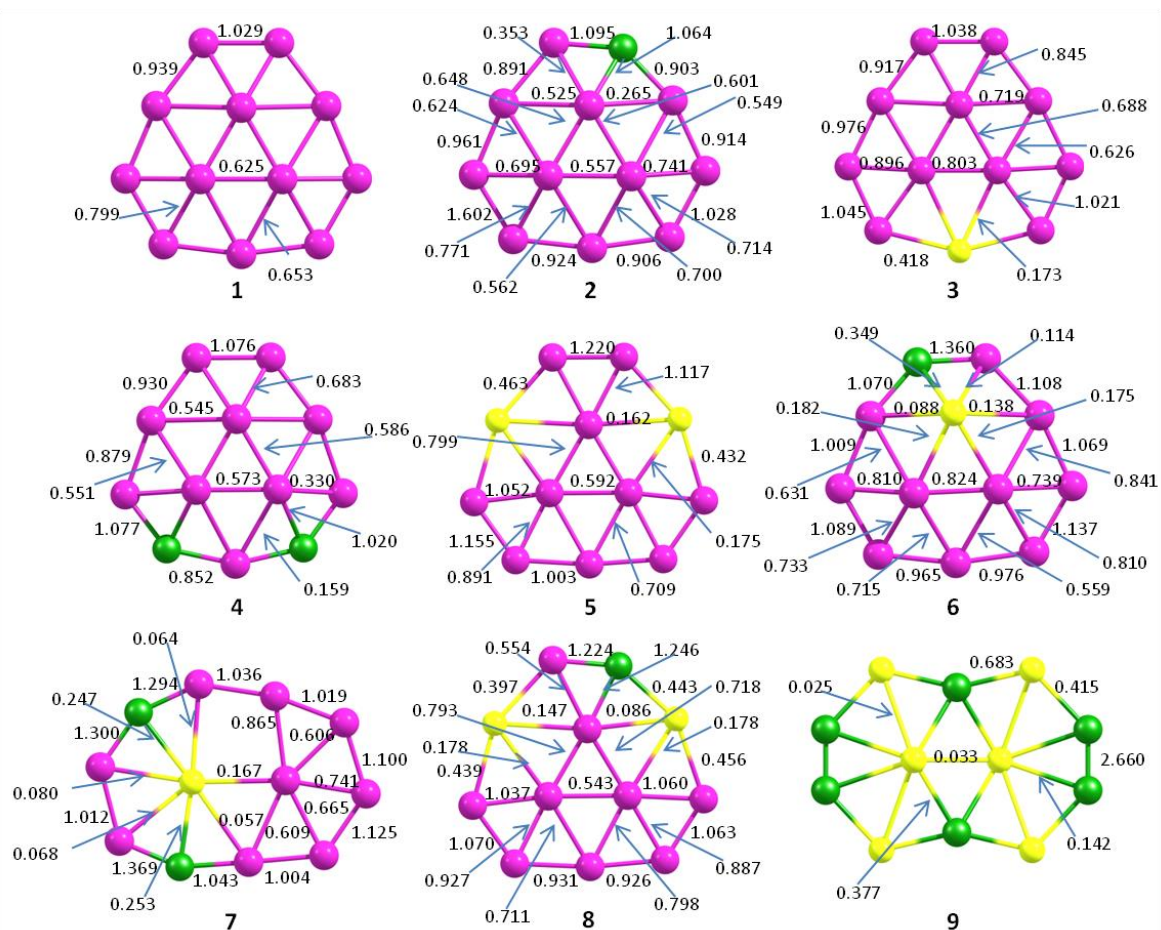
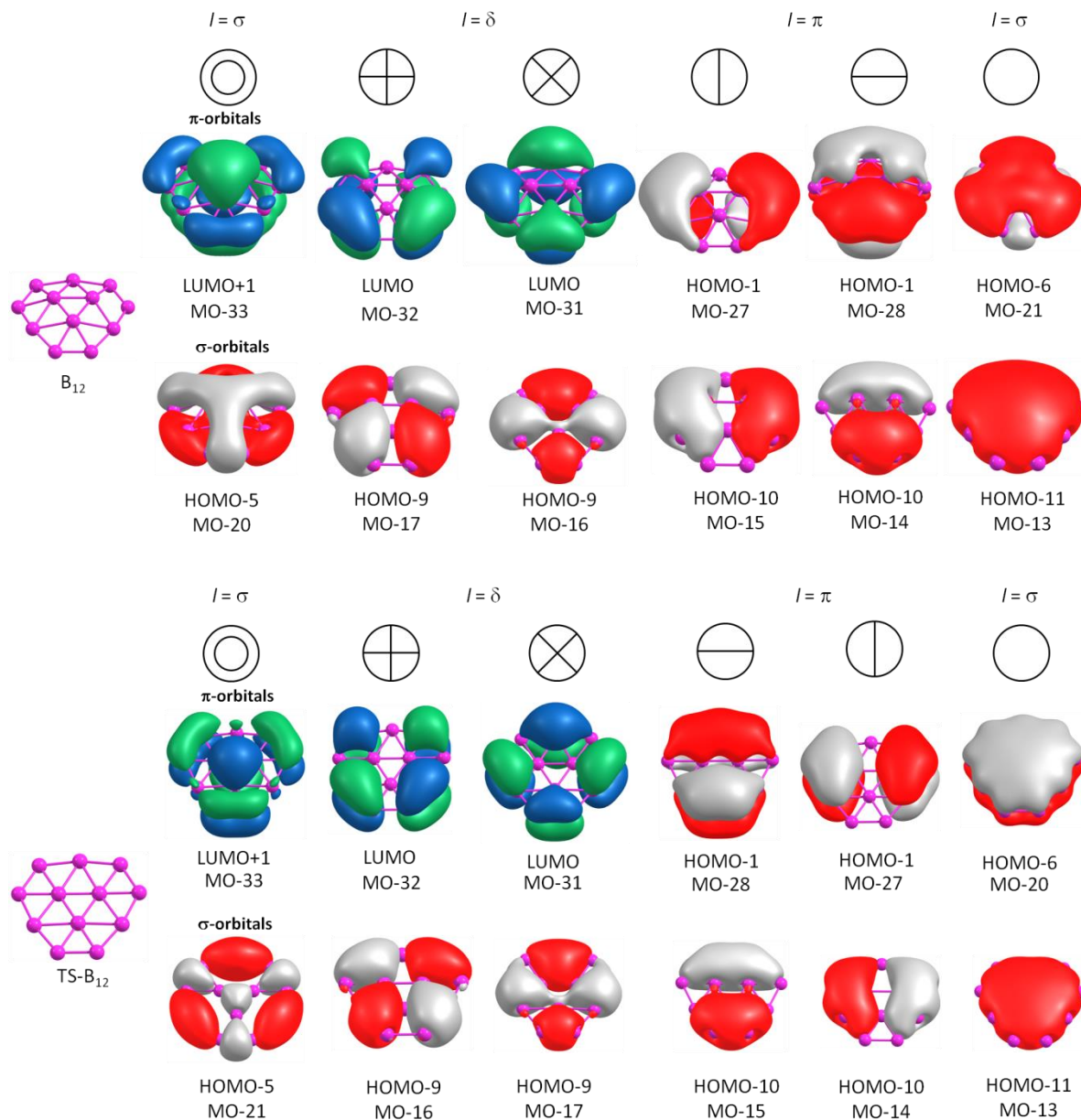


**Figure 6.** Delocalization indices (DI) values (in a.u.) for all the bonds of systems under analysis. Pink, yellow, and green spheres represent boron, beryllium, and carbon atoms, respectively.

### 3.3. Aromaticity

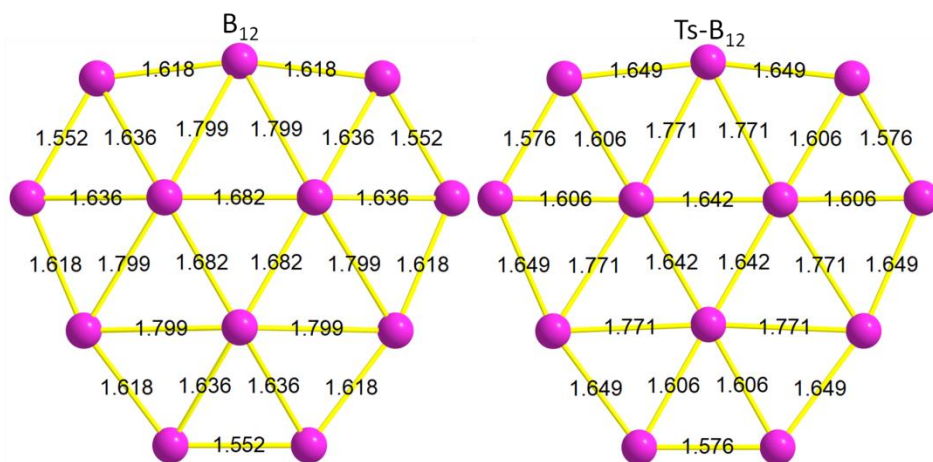
#### 3.3.1. Molecular orbitals

The computed **1**'s canonical molecular orbitals are in good agreement with Yuan's work.<sup>51</sup> The depicted orbitals contain the 6 delocalized  $\pi$ -electrons in a  $(1\sigma)^2(1\pi)^4$  electron configuration. The frontier molecular orbitals look very similar to those found in the  $(1\sigma)^2(1\pi)^4(1\delta)^4(2\sigma)^2$  configuration of disk aromatic species  $B_{19}^-$  and  $B_{20}^{2-}$ ,<sup>52</sup> and the recently reported  $B_{19}Si^-$  (isoelectronic to  $B_{20}^{2-}$ ).<sup>53</sup> In the Figure 7, the molecular orbitals of  $B_{12}$  and its planar transition state (TS- $B_{12}$ ) are depicted. In the picture were plotted the 6  $\pi$  electrons  $[(1\sigma)^2(1\pi)^4]$  and the 12 delocalized  $\sigma$  orbitals  $[(1\sigma)^2(1\pi)^4(1\delta)^4(2\sigma)^2]$ . The orbital occupation ( $\sigma$  and  $\pi$ ) could be associated with those compounds with disk-aromaticity. The DI calculations depicted in Figure 6, show values of 0.625 (a.u.) for the 3 inner boron atoms' bonds, this is an indicative that the six electrons forming the central triangle are delocalized and they are not forming three 2c-2e bonds, as Kiran et al. mentioned in their work.



**Figure 7.** Canonical occupied molecular orbitals computed on  $B_{12}$  and its planar transition state (TS- $B_{12}$ ). These MOs are in good agreement with those reported for disk-aromatic compounds. The  $\pi$  and  $\sigma$  electrons are in  $(1\sigma)^2(1\pi)^4$  and  $(1\sigma)^2(1\pi)^4(1\delta)^4(2\sigma)^2$  electronic configurations, respectively.

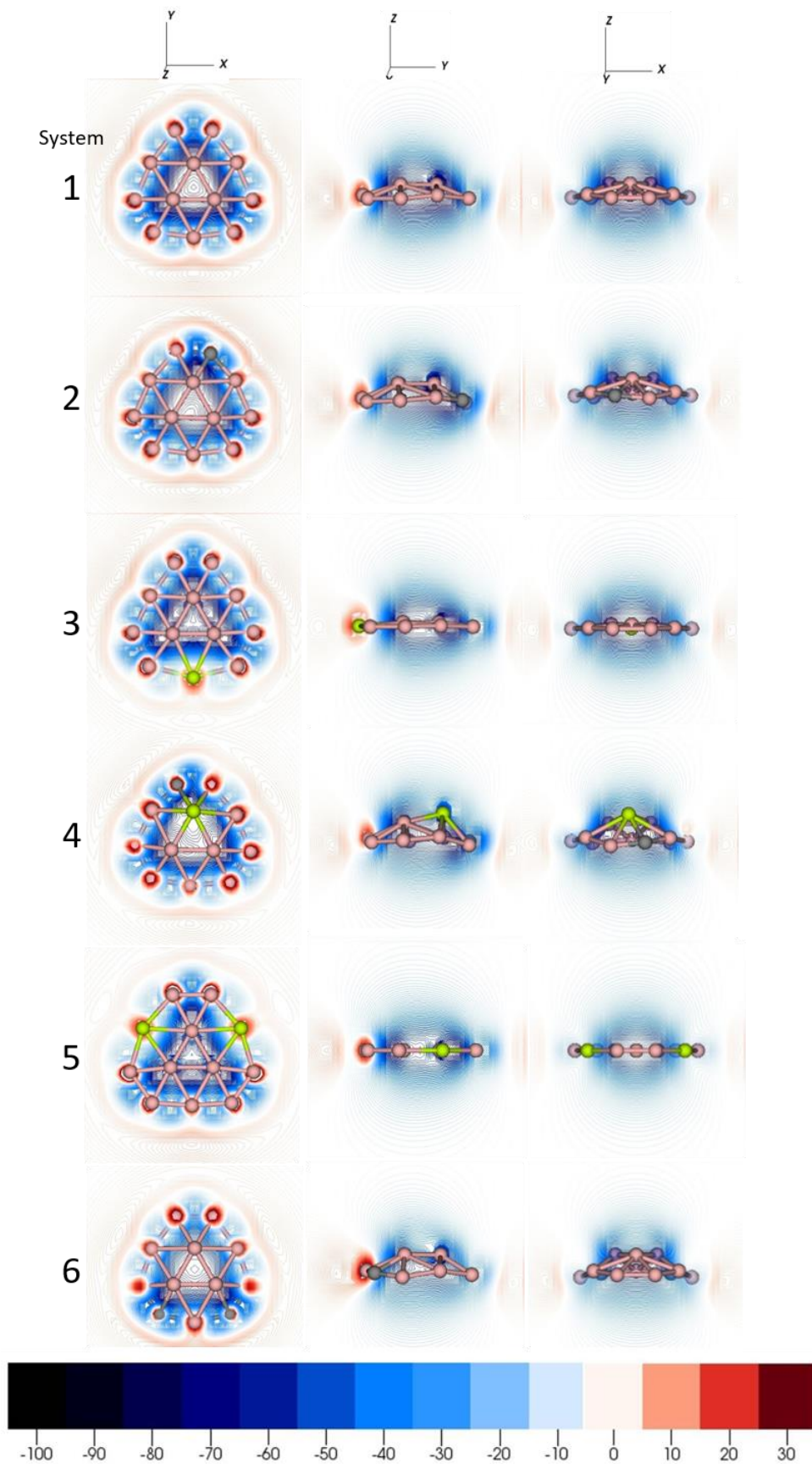
With the aim to confirm that these three MOs for B<sub>12</sub> are of  $\pi$ -type, we also calculated the planar geometry of B<sub>12</sub>, which corresponds to the transition state (TS) of the umbrella inversion of this system (Figure 7). The barrier only amounts to 4.5 kcal mol<sup>-1</sup>, and it is confirmed by one imaginary frequency that corresponds to the preference towards the bowl-shaped conformation, i.e. the equilibrium structure. The TS also presents three  $\pi$  MOs, thus confirming the above statement regarding the disk aromaticity for B<sub>12</sub>. Then, why does B<sub>12</sub> prefer not to be planar with the consequent loss of aromaticity? The answer must be found in the change of B-B bond lengths from bowl-shaped to planar conformations (Figure 8). The loss of aromaticity is compensated by stronger B-B bonds in the exterior ring, as observed for the slightly shorter bond lengths in non-planar B<sub>12</sub>. Then, both the bond lengths of the inner three-membered ring and those connecting the external and the inner ring become slightly longer in B<sub>12</sub> as compared to TS-B<sub>12</sub>.



**Figure 8.** Bond lengths (in Å) of bowl-shaped equilibrium structure of B<sub>12</sub> and its planar transition state.

### 3.3.2. Induced Magnetic Field ( $B^{\text{ind}}$ )

For a deeper understanding of the electronic delocalization, the induced magnetic field was calculated in all the compounds proposed in the current work, with that for **1** employed as reference. In Figure 9, the isolines of the z-component of the induced magnetic field ( $B^{\text{ind}}_z$ ) are plotted in different molecular orientations for a better appreciation of the isolines maps. Cluster **1** could be classified as a diatropic-response compound, as negative  $B^{\text{ind}}_z$  values are associated with aromatic compounds such as benzene.<sup>54</sup> The also bowl-shaped compounds **2**, **4**, and **6** present a comparable magnetic response, and the same happens for the planar structures **3**, **5**, **7**, and **8**. System **7**, which structurally is different to other GM, presents a strong diatropic region (aprox. -100 ppm) around the central boron atom, and another diatropic region (-60 ppm) around the two carbon atoms. So, cluster **7** could also be considered as a diatropic compound. On the other hand, cluster **8** is locally aromatic around the ring formed by six B and one Be. Finally, **9** (the boron-free compound) presents localized regions, with a diatropic region between the carbons in the CC units, and also the alone carbon atoms are surrounded by a localized diatropic region. On the other hand, the beryllium atoms are surrounded by localized paratropic regions. This magnetic response was previously observed in some systems such as “low delocalized” borazine.<sup>55</sup> With this magnetic response together with its non-planar structure, **9** could be classified as a non-aromatic compound.



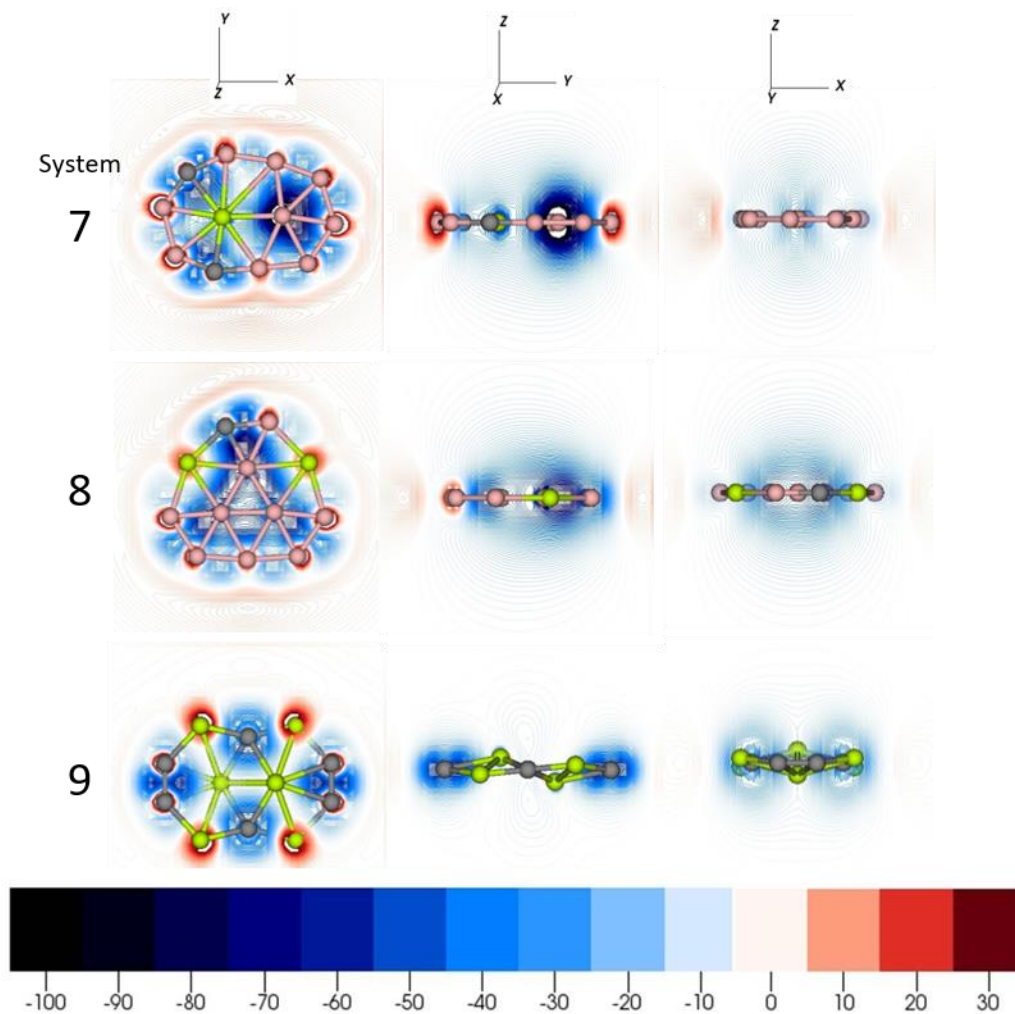


**Figure 9.** The  $z$ -component of the induced magnetic field ( $B_z^{\text{ind}}$ ) was computed assuming an external field  $B^{\text{ext}} = 1.0$  T. The units of the  $B_z^{\text{ind}}$  were ppm. Negative and positive values of the  $B_z^{\text{ind}}$  were related with diatropic (aromatic) and paratropic (antiaromatic) magnetic responses, respectively. Different planes (Cartesian  $yx$ ,  $yz$  and  $xz$ ) were plotted for a better inspection.  $B_{12}$ , labeled as **1**, was also analyzed.

### 3.3.3. Electron Localization Function (ELF)

The ELF provides deeper insight into nature of the chemical bonding.<sup>10, 56-57</sup> The topological analysis of this function presents a clear picture of bonding which could be rationalized through the interpretation of basins bifurcations. The ELF analysis has been carried out for classic examples such as benzene.<sup>58</sup> According to that work, the plotting at low values of ELF shows a single isosurface covering the full system. By increasing the ELF value this single isosurface splits into several ones, generating the basin bifurcation. The analysis of the ELF values separated in  $\sigma$ - $\pi$  orbital contributions has been proven to provide useful information about the degree of electron delocalization on aromatic systems.<sup>59</sup> In particular, systems with considerable degree of  $\pi$  electron delocalization show high bifurcation values for the  $ELF_{\pi}$ , above 0.7, in comparison to those systems with low degree,<sup>59</sup> with values around 0.3 or below. This fact can be used as a criterion to determine the aromatic character of the compounds. In the current work, ELF was computed only for systems with planar geometry: **3**, **5**, **7**, and **8**. The isosurface with  $ELF_{\pi}$  values of 0.3 and 0.7 in addition to that ELF value at which the bifurcation occurs are shown in Figure 10. The bifurcation values were higher than 0.7 suggesting that the four systems had a considerable degree of  $\pi$  electron delocalization.

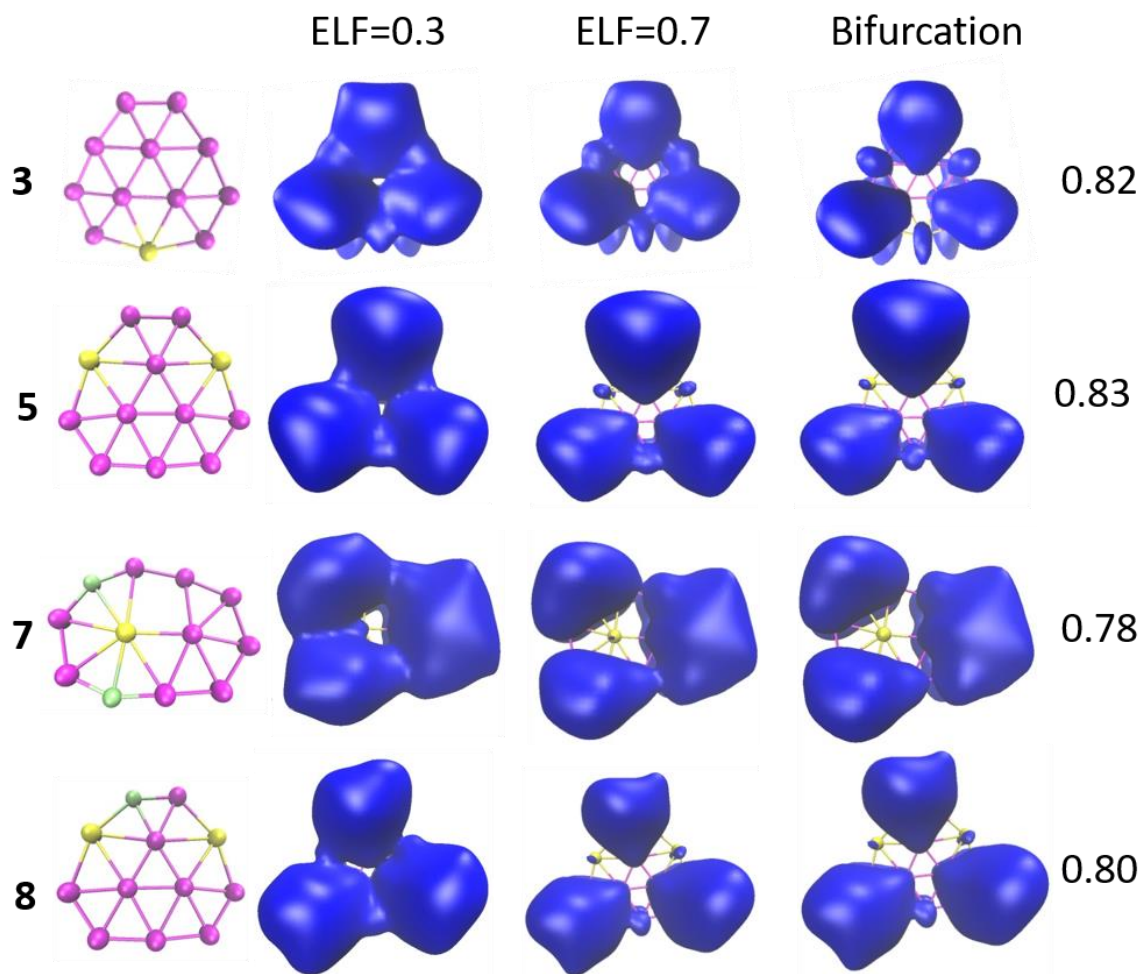


**Figure 10.** Isosurfaces of ELF computed in planar analogues **3**, **5**, **7**, and **8**. The third column titled “Bifurcation” shows the ELF’s bifurcation values for planar systems. Bifurcation values higher than 0.7, could be associated to delocalized systems, such as, benzene.

### 3.3.4. Multicenter Index of Aromaticity (MCI)

The multicenter index (MCI) accounts for the simultaneous electron sharing of various centers. The MCI of all rings of species **1** to **9** are gathered in Figure 11. As a measure of global electronic delocalization and, therefore, aromaticity, one can sum the MCI values for all the rings of a given system ( $\Sigma\text{MCI}_{3/4}$ ). If we do so, we obtain the following values for systems **1** to **9** in numerical order: 2.521, 2.178, 2.361, 1.860, 2.156, 1.776, 1.058, 1.952 and 0.380 e. From these numbers, we can derive the following conclusions: i) As expected,  $\Sigma\text{MCI}_{3/4}$  decreases when the number of substituted atoms increases; ii) substitution by  $\text{Be}^-$  affects the aromaticity less than substitution by  $\text{C}^+$  (compare **2** and **3** or **4** and **5**), which is likely due to the fact that  $\text{C}^+$  localizes the electron better than  $\text{Be}^-$ ; iii) for all systems, the electronic delocalization is more important in the unsubstituted regions; iv) the largest aromaticity is found in the unsubstituted **1** species and the lowest in the totally substituted  $\text{C}_6\text{Be}_6$  system that has to be considered nonaromatic; v) In **7**, there is an island of aromaticity around the  $\text{B}_6$  ring in agreement with the  $\text{B}_z^{\text{ind}}$  plot of Figure 9 and the ELF analysis of Figure 10 .

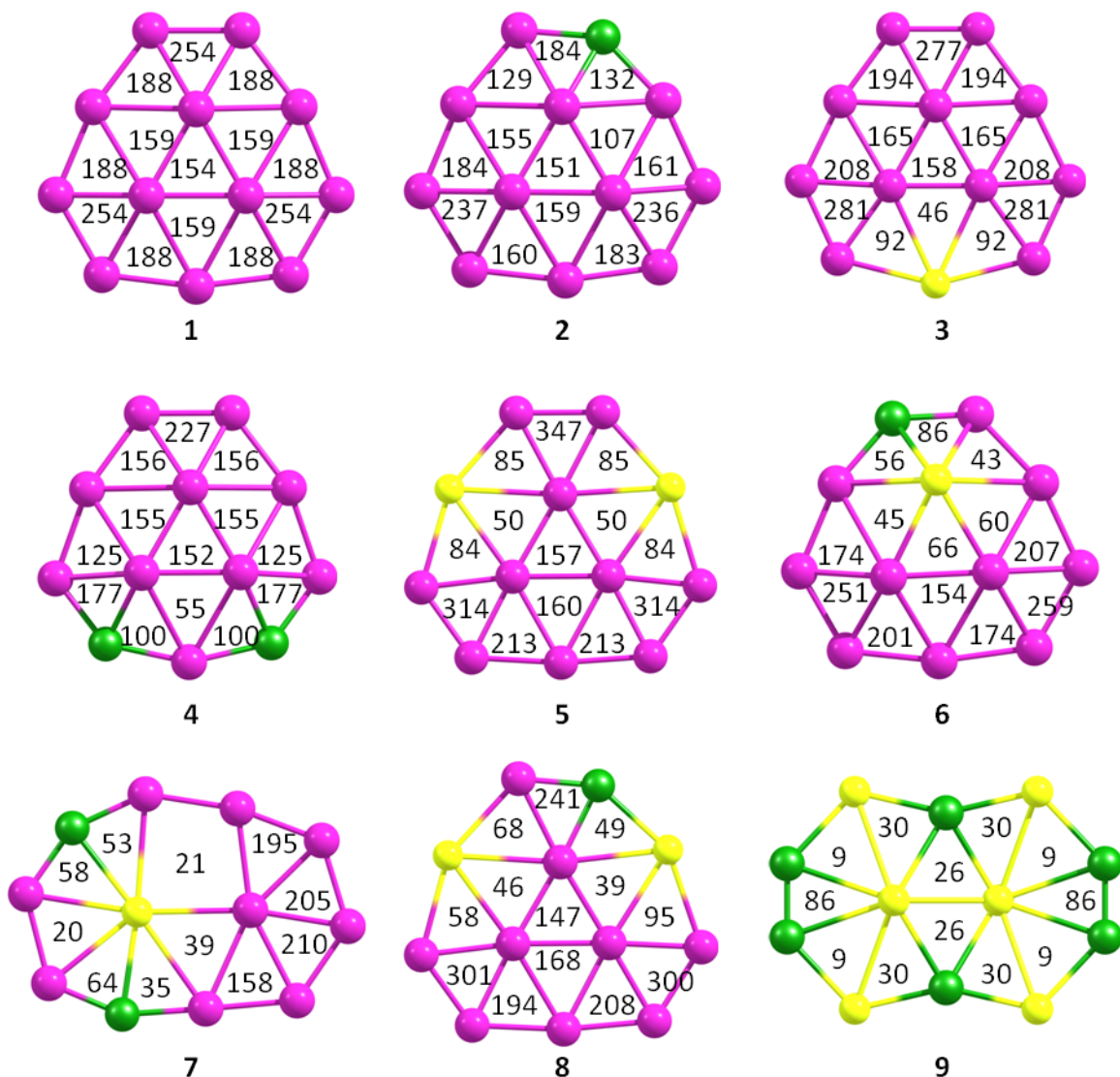


**Figure 11.** MCI values (in  $e \cdot 10^{-3}$ ) for all rings of systems under analysis. Pink, yellow, and green spheres represent boron, beryllium, and carbon atoms, respectively.

The MCI was computed on the **1**'s planar transition state (TS-B<sub>12</sub>) and the values are depicted in Figure 12. Not unexpectedly, the TS-B<sub>12</sub> has slightly higher MCI values than B<sub>12</sub>. For TS-B<sub>12</sub>, MCI can be dissected in the  $\sigma$  and  $\pi$  contributions ( $MCI = MCI_{\sigma} + MCI_{\pi}$ ), for a better understanding of the role of the two subsystems in the electronic delocalization. The  $\pi$  contribution indicates a high electronic delocalization of the  $\sigma$  electrons, but this is the result

of having 12  $\sigma$  delocalized electrons and only 6  $\pi$ . As a whole, we classify  $B_{12}$  as a double ( $\sigma$  and  $\pi$ ) disk aromatic compound.

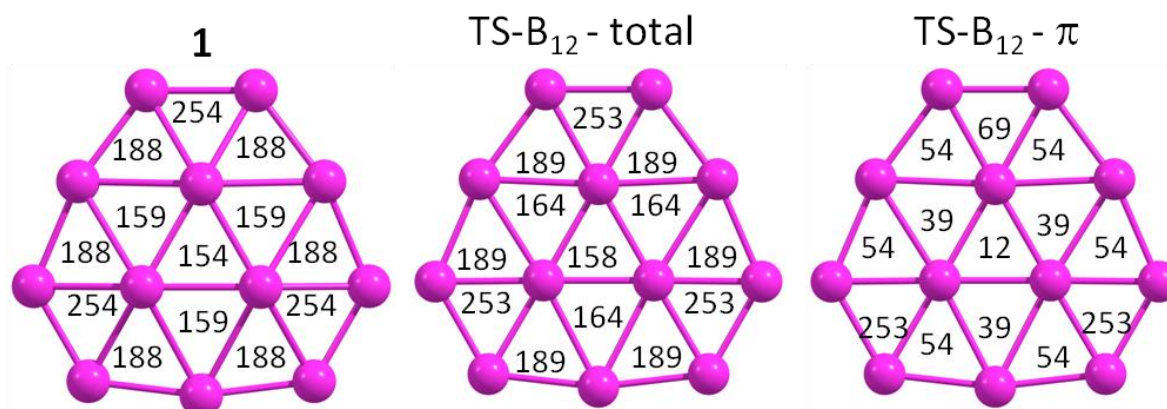


**Figure 12.** MCI values (in  $e \cdot 10^{-3}$ ) for **1** and its transition state (TS-B<sub>12</sub>). For TS-B<sub>12</sub> the separation of the  $MCI_{\pi}$  orbital contribution is also given ( $MCI = MCI_{\sigma} + MCI_{\pi}$ ).

### 3.3.5 Magnetically induced current density (MICD)

Only the planar systems (**3**, **5**, **7**, and **8**) were analysed with MICD methodology. In this section, **8** is employed as explained example. This system exhibits diatropic current in the inner part as well as outside the molecule (Figure 13, Left). This diatropic current is associated with an aromatic response when an external magnetic field is applied. The diatropic current is still present at  $1 a_0$  from the molecular plane (Figure 13, Right), and we can see the current flowing above the molecule.

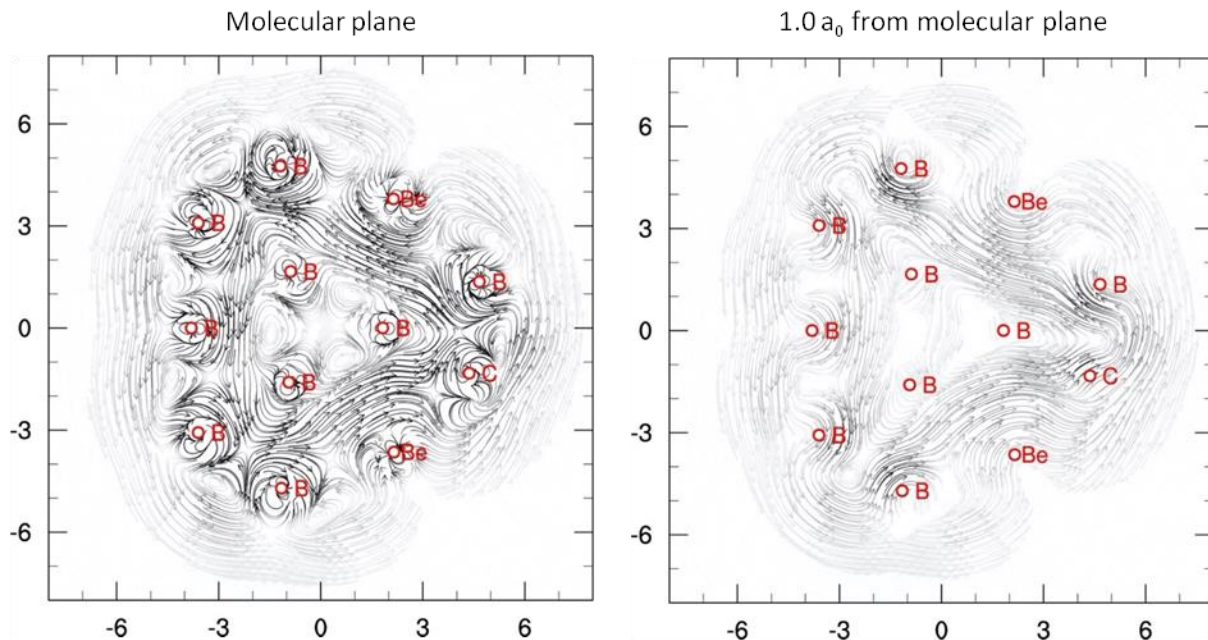


**Figure 13.** Magnetically Induced Current Density for **8** system. Left: MICD plotted at molecular plane and right: MICD placed at  $1.0 a_0$  from molecular plane. Line intensity is proportional to the norm of the current density vector. Diatropic current goes in counter-clockwise direction. The dimensions are  $16 \times 16 a_0$ .

Furthermore, the current density can be split between its diamagnetic and paramagnetic components. As expected, the diamagnetic components have diatropic behaviour, while the paratropic components have paramagnetic behaviour, as shown in Figure 14. The paramagnetic part does not present a homogeneous current, i.e., there are ring currents in the  $B_2Be$  and  $B_3$  rings in the molecular centre; nevertheless, the diamagnetic component is stronger than the paramagnetic one, resulting in a total diatropic current.

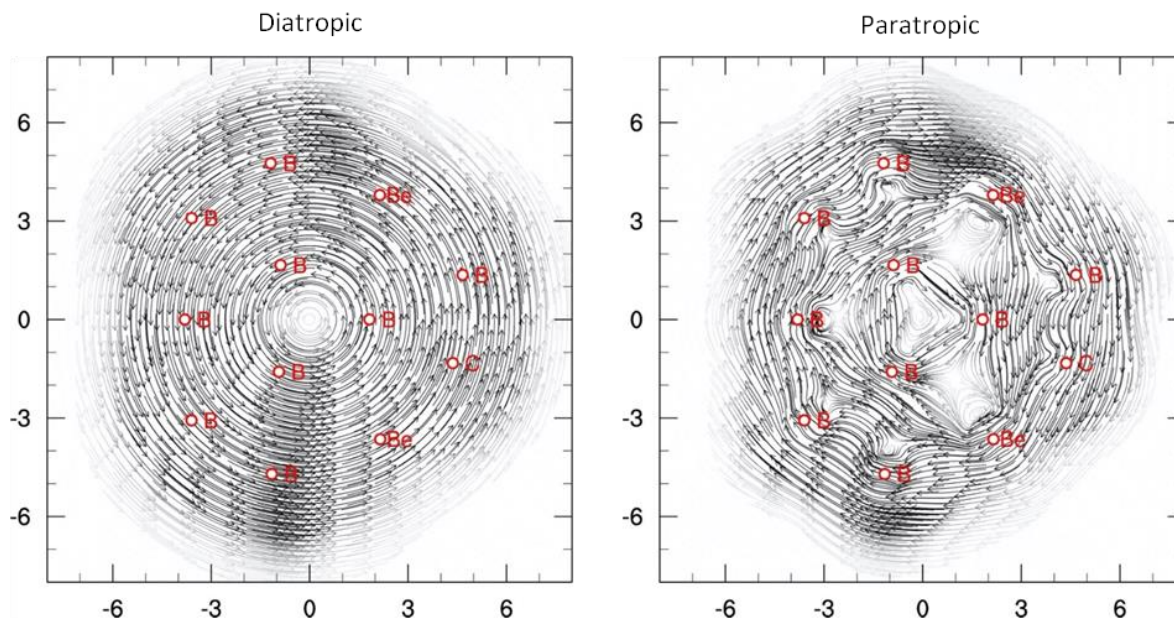


**Figure 14.** Left: diatropic component and right: paratropic component from the total MICD. Same convention used as in Figure 13.

For non-planar molecules, there are not local paratropic currents in molecular structures. Besides, as planar molecules, all systems present diatropic currents inside, as well as outside of the rings. All of them have aromatic behaviour based on the diatropic response of the MICD. The MICD plots for this set of molecules are cross-sections parallel to the  $B_3$  ring. These cross-sections go from minus  $2 a_0$  to  $2 a_0$  above the  $B_3$  ring. The plots are presented in SI together with diamagnetic and paramagnetic components of MICD.

The strength of this current density is integrated in a  $15 \times 15 a_0$  plane placed at the molecular centre. Figure 15 shows that MICD always exhibit a diatropic behaviour where the total strength of the current density for all planar molecules are bigger than benzene value (i.e.,  $9.56 \text{ nA/T}$ ). Due to symmetry conditions, the strength of the MICD is only evaluated in planar molecules where the plane does not bisect atoms, it is due that core electrons contribute with diamagnetic values to the magnetic.<sup>60</sup> Here is evident in the shoulders (interaction between

two atoms) from Figure 15. Unfortunately, this condition does not exist in non-planar molecules.

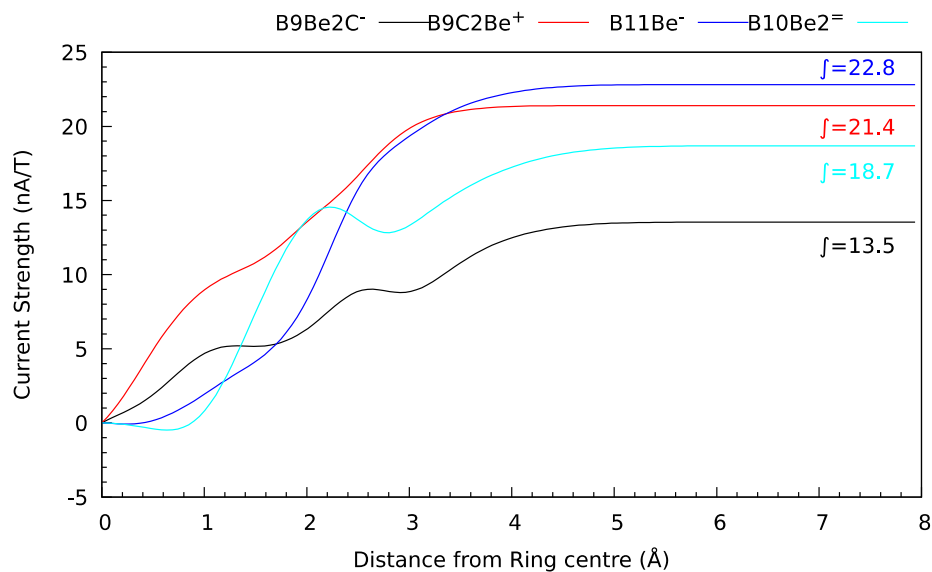


**Figure 15.** Strength of the current density as a function of the position from molecular centre to outside the molecule up to  $15a_0$ .

#### 4. Conclusions

Electronic transmutation states that an element, such as carbon, can behave structurally like boron if you make them valence isoelectronic, so C behaves as B if you remove one electron from its valence shell, generating  $C^+$ . One expects that the electronic transmuted compounds will show similar properties to the original ones. In this work, we have analyzed the single, double, and triple electronic transmutation of  $B_{12}$  with  $Be^-$  and  $C^+$ . Our aim is to find whether transmutation of B by  $Be^-$  modifies the properties of the original system to a more or less extent than substitution by  $C^+$ .

The isoelectronic substitutions revealed that  $Be^-$  changes the  $B_{12}$  bowl-shaped structure to planar (isomers **3** and **6**). On the other hand, the carbon atoms did not impact the original bowl-shaped structure (isomers **2** and **5**). When a “beryllium and carbon” double substitution

was done, the analogues showed similar tendency. For example, isomers **7** and **8** were planar but the first one had two beryllium atoms and the second one had just one beryllium. In all global minima of compounds with carbon atom(s), this atom was placed on the external ring, whereas beryllium atoms can be located both in the internal and external rings.

The impact of transmutation on the molecular structure can be associated to the electronic nature of beryllium and carbon ions. The carbon cation,  $C^+$ , is more electronegative than  $Be^-$ , for hence,  $C^+$  prefers to form localized bonds as those present in the external ring frame. The DI values support the bond order formed by the carbon atom. The bond length difference between C-B versus Be-B bonds makes the Be-doped structures' rings more flexible, allowing the planarity (for example, in **2**, the B-C are in the range of 1.424-1.483 Å meanwhile **3**'s Be-B bond is 1.856 Å).

Magnetically, all these 36-electrons compounds present a diatropic response similar to the original  $B_{12}$  cluster (except **9**). These results as well as the analysis of the MCI and the plots of  $ELF_\pi$  and MICS suggest that they are aromatic-like compounds (with the exception of  $Be_6C_6$ ). For  $B_{12}$ , there are 18-electrons that account for 2c-2e B-B bonds between the external B atoms of the ring (9 bonds), whereas 12  $\sigma$  and 6  $\pi$  electrons are delocalized over the disk giving rise to  $\sigma$  and  $\pi$  double disk aromaticity. Since all studied systems are isoelectronic, this disk aromaticity remains with single and double isoelectronic substitutions. However, substitution by  $Be^-$  affects the aromaticity less than substitution by  $C^+$ .

As a whole, substitution of B by  $Be^-$  has an important effect in the molecular structure that becomes planar but not in the aromaticity that is reduced only to a small extent.

## Acknowledgments

RI is grateful with Fondecyt 11160927 and Fondecyt 1201436 projects for the financial supporting. DI is grateful for the financial support by CONICYT PFCHA/DOCTORADO NACIONAL/2019 – 21190427. BZ-G acknowledges the financial support given by Conacyt Project (258647). This work has also been supported by the Ministerio de Economía y Competitividad (MINECO) of Spain (Projects CTQ2017-85341-P, CTQ2016-77558-R, and MDM-2017-0767) and the Generalitat de Catalunya (projects 2017SGR39 and 2017SGR348, Xarxa de Referència en Química Teòrica i Computacional, and ICREA Academia 2014 prize for M.S.). Excellent service by the Supercomputer center of the Consorci de Serveis Universitaris de Catalunya (CSUC) is gratefully acknowledged.

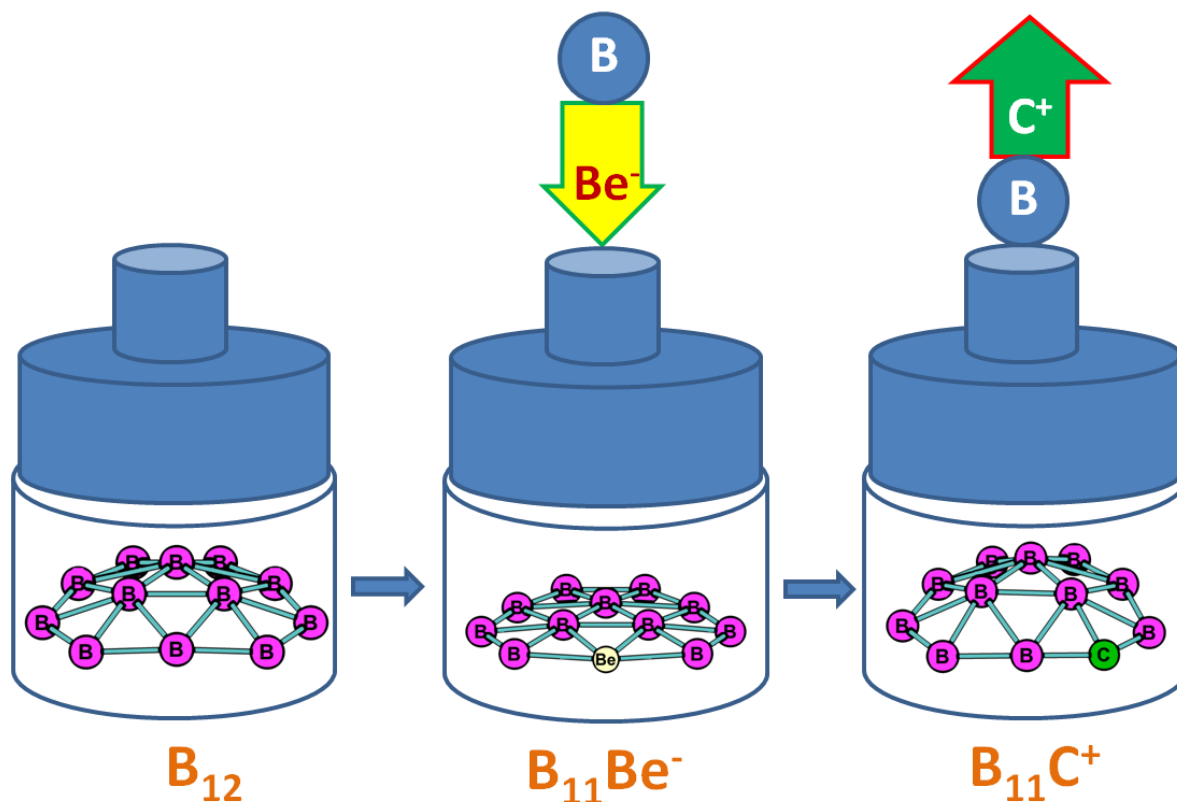
## 5. References

1. L. Hanley, J. L. Whitten and S. L. Anderson, *J. Phys. Chem.*, 1988, **92**, 5803-5812.
2. B. Kiran, G. Gopa Kumar, M. T. Nguyen, A. K. Kandalam and P. Jena, *Inorg. Chem.*, 2009, **48**, 9965-9967.
3. J. O. C. Jiménez-Halla, R. Islas, T. Heine and G. Merino, *Angew. Chem. Int. Ed.*, 2010, **49**, 5668-5671.
4. S. Jalife, L. Liu, S. Pan, J. L. Cabellos, E. Osorio, C. Lu, T. Heine, K. J. Donald and G. Merino, *Nanoscale*, 2016, **8**, 17639-17644.
5. R. Puchta, *Nat. Chem.*, 2011, **3**, 416.
6. X.-F. Zhao, J.-J. Li, H.-R. Li, C. Yuan, X. Tian, S.-D. Li, Y.-B. Wu, J.-C. Guo and Z.-X. Wang, *Phys. Chem. Chem. Phys.*, 2018, **20**, 7217-7222.
7. J. K. Olson and A. I. Boldyrev, *Chem. Phys. Lett.*, 2012, **523**, 83-86.
8. J. Poater, M. Solà, C. Viñas and F. Teixidor, *Chem. Eur. J.*, 2013, **19**, 4372-4372.
9. R. Islas, T. Heine and G. Merino, *Acc. Chem. Res.*, 2012, **45**, 215-228.
10. A. Savin, R. Nesper, S. Wengert and T. F. Fassler, *Angew. Chem., Int. Ed. Engl.*, 1997, **36**, 1809-1832.
11. P. Bultinck, R. Ponec and S. Van Damme, *J. Phys. Org. Chem.*, 2005, **18**, 706-718.
12. F. Feixas, E. Matito, J. Poater and M. Solà, *Chem. Soc. Rev.*, 2015, **44**, 6434-6451.
13. M. Giambiagi, M. S. de Giambiagi, C. D. dos Santos and A. P. de Figueiredo, *Phys. Chem. Chem. Phys.*, 2000, **2**, 3381-3392.
14. R. Islas, T. Heine, K. Ito, P. v. R. Schleyer and G. Merino, *J. Am. Chem. Soc.*, 2007, **129**, 14767-14774.
15. R. Islas, J. Poater, E. Matito and M. Solà, *Phys. Chem. Chem. Phys.*, 2012, **14**, 14850-14859.
16. D. Moreno, S. Pan, L. L. Zeonjuk, R. Islas, E. Osorio, G. Martínez-Guajardo, P. K. Chattaraj, T. Heine and G. Merino, *Chem. Commun.*, 2014, **50**, 8140-8143.
17. R. Islas, J. Poater and M. Solà, *Organometallics*, 2014, **33**, 1762-1773.
18. A. Vásquez-Espinal, J. Poater, M. Solà, W. Tiznado and R. Islas, *New J. Chem.*, 2017, **41**, 1168-1178.
19. R. Grande-Aztatzi, J. L. Cabellos, R. Islas, I. Infante, J. M. Mercero, A. Restrepo and G. Merino, *Phys. Chem. Chem. Phys.*, 2015, **17**, 4620-4624.
20. A. N. Alexandrova and A. I. Boldyrev, *J. Chem. Theor. Comp.*, 2005, **1**, 566-580.

21. J. P. Perdew, K. Burke and M. Ernzerhof, *Phys. Rev. Lett.*, 1996, **77**, 3865-3868.
22. J. P. Perdew, K. Burke and M. Ernzerhof, *Phys. Rev. Lett.*, 1997, **78**, 1396-1396.
23. F. Weigend and R. Ahlrichs, *Phys. Chem. Chem. Phys.*, 2005, **7**, 3297-3305.
24. K. Raghavachari, G. W. Trucks, J. A. Pople and M. Head-Gordon, *Chem. Phys. Lett.*, 1989, **157**, 479-483.
25. T. J. Lee and P. R. Taylor, *Int. J. Quantum Chem.*, 1989, **36**, 199-207.
26. M. J. Frisch, G. W. Trucks, H. B. Schlegel, G. E. Scuseria, M. A. Robb, J. R. Cheeseman, G. Scalmani, V. Barone, B. Mennucci, G. A. Petersson, H. Nakatsuji, M. Caricato, X. Li, H. P. Hratchian, A. F. Izmaylov, J. Bloino, G. Zheng, J. L. Sonnenberg, M. Hada, M. Ehara, K. Toyota, R. Fukuda, J. Hasegawa, M. Ishida, T. Nakajima, Y. Honda, O. Kitao, H. Nakai, T. Vreven, J. J. A. Montgomery, J. E. Peralta, F. Ogliaro, M. Bearpark, J. J. Heyd, E. Brothers, K. N. Kudin, V. N. Staroverov, T. Keith, R. Kobayashi, J. Normand, K. Raghavachari, A. Rendell, J. C. Burant, S. S. Iyengar, J. Tomasi, M. Cossi, N. Rega, J. M. Millam, M. Klene, J. E. Knox, J. B. Cross, V. Bakken, C. Adamo, J. Jaramillo, R. Gomperts, R. E. Stratmann, O. Yazyev, A. J. Austin, R. Cammi, C. Pomelli, J. W. Ochterski, R. L. Martin, K. Morokuma, V. G. Zakrzewski, G. A. Voth, P. Salvador, J. J. Dannenberg, S. Dapprich, A. D. Daniels, O. Farkas, J. B. Foresman, J. V. Ortiz, J. Cioslowski and D. J. Fox, *Gaussian 09 Revision D.01*, Gaussian Inc. Wallingfor CT, 2013.
27. A. M. Koster, G. Geudtner, A. Alvarez-Ibarra, P. Calaminici, M. E. Casida, J. Carmona-Espindola, V. D. Dominguez, R. Flores-Moreno, G. U. Gamboa, A. Goursot, T. Heine, A. Ipatov, A. d. l. Lande, F. Janetzki, J. M. d. Campo, D. Mejia-Rodriguez, J. U. Reveles, J. Vasquez-Perez, A. Vela, B. Zuniga-Gutierrez and D. R. Salahub, *deMon2k*, Cinvestav, Mexico City, 2016.
28. H. Childs, E. Brugger, B. Whitlock, J. Meredith, S. Ahern, D. Pugmire, K. Biagas, M. Miller, C. Harrison, G. H. Weber, H. Krishnan, T. Fogal, A. Sanderson, C. Garth, E. W. Bethel, D. Camp, O. Rubel, M. Durant, J. M. Favre and P. Navratil, *High Performance Visualization--Enabling Extreme-Scale Scientific Insight*, 2012, pp 357-372.
29. T. Lu and F. Chen, *J. Comput. Chem.*, 2012, **33**, 580-592.
30. T. Saue, *ChemPhysChem*, 2011, **12**, 3077-3094.
31. E. Matito, P. Salvador, M. Duran and M. Solà, *J. Phys. Chem. A*, 2006, **110**, 5108-5113.
32. E. Matito, *Journal, ESI-3D: Electron Sharing Indexes Program for 3D Molecular Space Partitioning*, Girona, 2014. Available from <http://iqc.udg.es/~eduard/ESI>.
33. E. Matito, M. Duran and M. Solà, *J. Chem. Phys.*, 2005, **122**, 14109.
34. E. Matito, F. Feixas and M. Solà, *J. Mol. Struct-THEOCHEM*, 2007, **811**, 3-11.
35. A. S. P. Gomes, T. Saue, L. Visscher, H. J. A. Jensen, R. Bast, I. A. Aucar, V. Bakken, K. G. Dyall, S. Dubillard, U. Ekström, E. Eliav, T. Enevoldsen, E. Faßhauer, T. Fleig, O. Fossgaard, L. Halbert, E. D. Hedegård, T. Helgaker, B. Helmich-Paris, J. Henriksson, M. Iliaš, C. R. Jacob, S. Knecht, S. Komorovský, O. Kullie, J. K. Lærdahl, C. V. Larsen, Y. S. Lee, H. S. Nataraj, M. K. Nayak, P. Norman, G. Olejniczak, J. Olsen, J. M. H. Olsen, Y. C. Park, J. K. Pedersen, M. Pernpointner, R. Di Remigio, K. Ruud, P. Sałek, B. Schimmelpfennig, B. Senjean, A. Shee, J. Sikkema, A. J. Thorvaldsen, J. Thyssen, J. van Stralen, M. L. Vidal, S. Villaume, O. Visser, T. Winther and S. Yamamoto, DIRAC: Program for Atomic and Molecular

- Direct Iterative Relativistic All-electron Calculations, 2017. DOI: 10.5281/zenodo.3572668.
36. A. D. Becke, *J. Chem. Phys.*, 1993, **98**, 5648-5652.
  37. C. Lee, W. Yang and R. G. Parr, *Phys. Rev. B*, 1988, **37**, 785-789.
  38. S. H. Vosko, L. Wilk and M. Nusair, *Can. J. Phys.*, 1980, **58**, 1200-1211.
  39. R. Bast, J. Jusélius and T. Saue, *Chem. Phys.*, 2009, **356**, 187-194.
  40. T. H. Dunning, *J. Chem. Phys.*, 1989, **90**, 1007-1023.
  41. B. P. Pritchard, D. Altarawy, B. Didier, T. D. Gibson and T. L. Windus, *J. Chem. Inf. Model.*, 2019, **59**, 4814-4820.
  42. See <http://www.pyngl.ucar.edu/> for *PyNGL*, developed at the National Center for Atmospheric Research.
  43. F. Cervantes-Navarro, G. Martínez-Guajardo, E. Osorio, D. Moreno, W. Tiznado, R. Islas, K. J. Donald and G. Merino, *Chem. Commun.*, 2014, **50**, 10680-10682.
  44. W. Huang, A. P. Sergeeva, H.-J. Zhai, B. B. Averkiev, L.-S. Wang and A. I. Boldyrev, *Nat. Chem.*, 2010, **2**, 202.
  45. D. Kang, W. Sun, H. Shi, C. Lu, X. Kuang, B. Chen, X. Xia and G. Maroulis, *Sci. Rep.*, 2019, **9**, 14367.
  46. B. B. Averkiev, D. Y. Zubarev, L.-M. Wang, W. Huang, L.-S. Wang and A. I. Boldyrev, *J. Am. Chem. Soc.*, 2008, **130**, 9248-9250.
  47. R. F. W. Bader, *Atoms in Molecules: A Quantum Theory*, Clarendon Press, 1994.
  48. Y.-J. Wang, X.-Y. Zhao, Q. Chen, H.-J. Zhai and S.-D. Li, *Nanoscale*, 2015, **7**, 16054-16060.
  49. J. Poater, M. Solà and F. M. Bickelhaupt, *Chem. Eur. J.*, 2006, **12**, 2889-2895.
  50. J. Poater, M. Solà and F. M. Bickelhaupt, *Chem. Eur. J.*, 2006, **12**, 2902-2905.
  51. Y. Yuan and L. Chen, *J. Chem. Phys.*, 2013, **138**, 024301.
  52. T. B. Tai, R. W. A. Havenith, J. L. Teunissen, A. R. Dok, S. D. Hallaert, M. T. Nguyen and A. Ceulemans, *Inorg. Chem.*, 2013, **52**, 10595-10600.
  53. D. T. Tuyet Mai, L. Van Duong, M. P. Pham-Ho and M. T. Nguyen, *J. Phys. Chem. C*, 2020, **in press**.
  54. T. Heine, R. Islas and G. Merino, *J. Comput. Chem.*, 2007, **28**, 302-309.
  55. R. Islas, E. Chamorro, J. Robles, T. Heine, J. C. Santos and G. Merino, *Struct. Chem.*, 2007, **18**, 833-839.
  56. A. D. Becke and K. E. Edgecombe, *J. Chem. Phys.*, 1990, **92**, 5397-5403.
  57. F. Feixas, E. Matito, M. Duran, M. Solà and B. Silvi, *J. Chem. Theor. Comp.*, 2010, **6**, 2736-2742.
  58. A. Savin, B. Silvi and F. Colonna, *Can. J. Chem.*, 1996, **74**, 1088-1096.
  59. J. C. Santos, W. Tiznado, R. Contreras and P. Fuentealba, *J. Chem. Phys.*, 2004, **120**, 1670-1673.
  60. D. Arias-Olivares, D. Páez-Hernández and R. Islas, *New J. Chem.*, 2018, **42**, 5334-5344.

## Table of Contents.



In the current work  $B \rightarrow Be^-$  and  $B \rightarrow C^+$  isoelectronic substitutions were carried out and a new set of molecules were proposed, and their stability was studied in terms of the electronic delocalization. The isoelectronic substitution  $B \rightarrow Be^-$  in  $B_{12}$  boron cluster generated a new planar global minimum:  $B_{11}Be^-$ . And the  $B \rightarrow C^+$  isoelectronic substitution generated the non-planar  $B_{11}C^+$ .

### RESPONSE TO REVIEWER 1

It is not explained why carbon enhances the bowl shape, while beryllium leads to pseudo-planarity. I suspect the reason is strain, related to the bond lengths.

**Answer:** As suggested by the Reviewer, we have added a new paragraph at the end of the 3.1. Structural Details section showing how substitution of B by  $C^+$  causes the new B-C bonds to be even shorter than the equivalent B-B bonds in  $B_{12}$ , thus keeping the bowl-shaped geometry. On the other hand, the substitution of B by  $Be^-$  causes an elongation of the new B-Be bonds compared to B-B in  $B_{12}$ , thus allowing a decrease of the strain which drives to a planar geometry. Planar geometry is preferred because it favors electron delocalization. However, if bonds are too short, then the bowl-shape geometry is unavoidable.

Nor is the coordination difference between C and Be well explained. Also if Be prefers hypercoordination, then why wants it to reside on the outer ring?

**Answer:** Related to the different coordination of C and Be, when we discuss the two-atom substitution, we already refer to a previous work by Boldyrev: "This result concurs with the previously reported finding by Boldyrev et al. that carbon tends to avoid hypercoordination in  $CB_6^-$ ,  $CB_6^{2-}$ , and  $C_2B_5^-$  planar carbon-boron clusters.<sup>46</sup>". In particular, we refer to that work based on the larger preference of C to be at an outer position rather than Be, a trend which is further supported in the beryllium-carbon cluster **9**, as pointed out in the manuscript. From the

analyzed compounds it is observed how in all minima, C is placed in the outer ring, whereas Be can be either located in the outer or inner rings. We clearly state that C wants to avoid hypercoordination, as well that it is known that Be in some compounds is hypercoordinated (reference 6). Furthermore, the preference of C for the outer ring can be further justified by its higher tendency to retain electrons (larger  $z$ ), thus driving to more localized bonds, at difference with Be that drives to more delocalized bonds. This trend can be perfectly observed by means of the delocalization indices enclosed in the topological analysis. For such, an extra paragraph has been introduced in p. 11 and in the Conclusions section.